Simulation of magnetic separation process in wet low intensity magnetic separator using DPM-CFD Method

Pouya Karimi[1], Zahra Mansourpour[2], Ahmad Khodadadi Darban[1]
1. Mineral Processing Dept., Tarbiat Modares University, Tehran, Iran
2. School of Chemical Engineering, College of Engineering, University of Tehran, Tehran, Iran

Journal of Advanced Environmental Research and Technology

Vol. 1, No.1
page 59-73 ,spring 2023
***
Received 5 Desember 2022
Accepted 30 February 2023

Abstract

Low Intensity Magnetic Separators (LIMS) are widely used in research and industry. The design of this separator is based on drum rotation inside a tank media, so that a permanent magnets placing inside the drum as an angle form, produces a magnetic field. In this study, the behavior of magnetic and none-magnetic particles of a pulp, flowing through a magnetic field in the wet LIMS, was simulated and validated by experimental results. The magnetic field variables were calculated in an FEM based simulator (COMSOL Multiphysics); while particles' tracking was done applying CFD numerical method, enhanced by discrete phase model (DPM). The difference between the results of the simulation and the magnetic separation experimental test (recovery of magnetic particles in the concentrate product) was 16.4%. In order to quantify the results of the simulation, magnetic separation simulation was performed by changing two variables affecting the magnetic separation process (variables of particle size of the input pulp feed particles and solid percentage of input pulp) and corresponding experiments. Comparison of laboratory and simulation results showed that the trend of simulation results is consistent with laboratory results of the weight recovery (in both variables under study), so that the maximum simulation error is related to the size of 125 microns (16.5 %) and the lowest simulation error was in 180 microns (11.4 %). Also, the lowest simulation error in the weight recovery prediction was related to the pulp feed solid percentage of 15% (equivalent to 14%) and the highest simulation error was in 30% pulp feed solid percentage (16.9 %). This proposes that FEM-DPM-CFD coupling model, can be applied for simulation, optimization, design and construct more advanced magnetic separators machines.

key words

Magnetic separation

wet LIMS

finite element method (FEM)

computational fluid dynamics (CFD)

discrete phase model (DPM)

*To whom correspondence should be addressed:
mansourp@ut.ac.ir

1. Introduction

Demand for effective, clean and simple separation techniques is increasing, while declining mineral resources and environmental restrictions have become more stringent. Since magnetic separation is clean and proceeds at numerous conditions, it has been preferred over other separation techniques in many situations [1] and has led to its unique position among separation technologies.

Magnetic separations have for decades been applicable processes in different industries ranging from steel production to coal desulfurization [2]. Magnetic separation has been used for separation of gangue from ore to enrich low grade ore [3, 4, 5, 6, 7 and 8], separation of magnetic from non-magnetic waste [9, 10], heavy media separation [11], separation of pyrite (FeS_2) from coal for desulfurization [2], Kaolin (clay) decolorization and remove ironic impurities [2, 12], processing a rare earth mineral deposit [13, 14], water treatment and metal removal [2], waste water treatment [15], food industry and remove rare earth elements [2], etc. Furthermore, in the field of biotechnology such as protein and DNA purification, cell separation, separation of biological cells and drug delivery [2, 10 and 16], and biocatalysis and diagnostics, magnetic separation has a wide range using.

According to the different parameters (consist of intensity of magnetic field, its gradient and dry or wet operation of the equipment), magnetic separators classified as Dry low-intensity magnetic separators, Wet low-intensity magnetic separators, Dry high-intensity magnetic separators, Wet high-intensity high-gradient magnetic separators and finally Eddy-current separators and separation in magnetic fluid [17]. In another classification, magnetic separation equipment for minerals processing generally falls into three basic categories: low, medium and high intensity, based on the relative magnetic field strength employed to accomplish separation [18]. By far the most frequently used wet low-intensity magnetic separators are drum separators [9, 19 and 20].

Despite its simple function, simulation of magnetic separation is complicated, as several liquid-liquid, solid-liquid, solid-solid forces act along with gravitational and magnetic forces. Computational Fluid Dynamic (CFD) has been found to be a useful tool for studying the behavior of the particles in the presence of a magnetic field [21]. Several studies have been carried out in recent years to simulate the magnetic separation process using the CFD approach, briefed in Table 1. Majority of these studies are related to design improvement and optimization of separation process in High-Gradient Magnetic Separators (HGMS) [1, 21, 22, 23, 24, 25 and 26]. This is while limited simulation studies were conducted for the wet LIMS device. In the first simulation study, the flow of materials in the LIMS device is simulated using the combination of FEM, CFD and DEM numerical methods [28]. In the latest study in 2019, the 2D dynamic behavior of magnetic particles in wet LIMS (counter-rotation type) was studied. In the mentioned study, particle tracing for fluid flow module is used to calculate the location and the dynamic behavior of particles under the magnetic and flow fields [29].

The first step in the simulating of magnetic separation process is to simulate the magnetic field and the corresponding variables. The most accurate numerical method for simulating magnetic variables is the finite element numerical method (FEM) [30, 31, 32, 33 and 34]. There are several available FEM base simulators such as: COMSOL Multiphysics, Opera, Faraday, EMAG, etc, which can be successfully used to calculate the magnetic field parameters [28]. In the following, simulation of pulp flow in a magnetic separator is performed using a CFD numerical method.

Here we study the flow behavior of the magnetic and non-magnetic particles affected by a magnetic field in wet LIMS equipment. In this retrieval, laboratory wet LIMS device was first disassembled and by using of the reverse engineering process, the mechanical and magnetic information of the magnets inside the drum was extracted. Then, magnetic variables of magnetic flux density (B) and magnetic field intensity (H) were simulated using finite element method (FEM). In the next step, the results of simulation and laboratory measurements (of the magnetic field) were compared to validate the results of the simulation. In the continue, fluid flow were simulated by CFD numerical methods. To quantify the results of the simulation, magnetic separation simulation was performed by changing two variables affecting the magnetic separation process, consist of particle size of the input pulp feed particles in four levels (+180, +125, +90 and +63 microns) and solid percentage of the input pulp in four levels (15, 20, 25 and 30 % by weight) and corresponding experiments. One of the objectives of this study is to investigate the feasibility of using the combination of FEM-CFD-DPM, as an

Table 1: List of recent studies on numerical simulation of magnetic separation

Magnetic separation equipment	Numerical method	Subject	Reference
HGMS	CFD (Eulerian–Lagrangian model)	Investigating the behavior of a magnetic separator.	[22]
HGMS	CFD (Eulerian–Lagrangian model)	Determining the separation efficiency of different wire arrangements.	[23]
HGMS	FEM-CFD (Lagrangian model)	Studying the particle trajectory by solving the equation of motion for a rectangular wire shape.	[24]
HGMS	CFD (Eulerian-Eulerian model)	Studying the flow behavior of particles and visualize the accumulation of magnetic particles on the magnetic plate.	[1]
HGMS	FEM-CFD-DEM	Examining the particle deposition on wires.	[25]
HGMS	CFD (Eulerian-Eulerian model)	Studying the trapping of particles in a matrix of paramagnetic spheres.	[21]
HGMS	FEM-CFD (Lagrangian model)	Calculating the trajectories of virtual magnetizable particles and quantifying the effects of the geometric variations.	[26]
Quadrupole Magnetic Sorter (QMS)	CFD (Eulerian model))	Investigating the flow behaviour and the effect of the splitter thickness on the nonspecific crossover.	[27]
Low Intensity Magnetic Separator (LIMS)	FEM-CFD-DEM	Investigating the flow behaviour and Slurry flow patterns in the LIMS	[28]
Wet LIMS	FEM-CFD	Investigate the 2D dynamic behavior of multi-type magnetic particles in counter-rotation (CR) type LIMS	[29]

Eulerian-Lagrangian method to simulate the magnetic separation process.

2. Modeling theory

2.1. Magnetic field simulation using FEM method

The basic equations for solving the magnetic field in COMSOL Multiphysics are based on equations 1 and 2 [35]:

$$\nabla(\mu_0 \mu_r H)=0 \quad (1)$$

$$H=-\nabla V_m+H_b \quad (2)$$

After calculating the magnetic field (H) in different directions, the magnetic field gradient was also calculated. The calculation of the magnetic field intensity gradient was based on Helmholtz model of Equation 3:

$$\nabla H=(\partial/\partial x,\partial/\partial y,\partial/\partial z)(H_x,H_y,H_Z)$$

$$\nabla H=\begin{bmatrix} \frac{\partial H_x}{\partial x} & \frac{\partial H_x}{\partial y} & \frac{\partial H_x}{\partial z} \\ \frac{\partial H_y}{\partial x} & \frac{\partial H_y}{\partial y} & \frac{\partial H_y}{\partial z} \\ \frac{\partial H_z}{\partial x} & \frac{\partial H_z}{\partial y} & \frac{\partial H_z}{\partial z} \end{bmatrix}=\begin{bmatrix} H_{xx} & H_{xy} & H_{xz} \\ H_{yx} & H_{yy} & H_{yz} \\ H_{zx} & H_{zy} & H_{zz} \end{bmatrix}$$

$$\nabla H_x=H_{xx}+H_{yx}+H_{zx}$$
$$\nabla H_y=Hxy+H_{yy}+H_{zy}$$
$$\nabla H_z=Hxz+H_{yz}+H_{zz} \quad (3)$$

2.2. Magnetic force of external magnetic field

The magnetic force acted on the particles carried by the fluid flow is a function of the magnitude of the magnetization of the particles and the gradient of the intensity of the magnetic field and it is calculated from equation (4). In equation 4, μ0 is the magnetic permeability coefficient in vacuum (equivalent to $4\pi\times10^{(-7)}$ Tm/A), Vm represents the volume of the particles, M is the mean magnetization (Am-1) and H is the magnetic field intensity (Am-1) and its gradient is in Am-2 [25,28 and 36]:

$$(F_M) = \mu_0 V_m M\nabla H \quad (4)$$

2.3. Discrete Phase Model (DPM)

Discrete Phase Model of Fluent uses the Eulerian-Lagrangian approach. The fluid phase is solved by the Navier-Stokes equation, while the discrete phase is calculated by tracking a number of particles. The motion path of the discrete phase is predicted by the total force balance, which in the Cartesian coordinates is shown in equation 5 [37]:

$$\frac{du_p}{d_t} = F_D(\vec{u} - \vec{u}_p) + \frac{\vec{g}(\rho_p - \rho)}{\rho_p} + \vec{F} \quad (5)$$

Where F_D $(u - u_p)$ represents the drag force, $(g(\rho_p-\rho))/\rho_p$ is related to the buoyancy force and F represents other forces acting on particles rather than the drag and the buoyancy forces, such as gravity and electromagnetic force. Drag force is calculated by equation 6:

$$F_D = \frac{18\mu}{\rho_p d_p^2}\frac{C_D Re}{24} \quad (6)$$

Where u is the velocity of fluid phase, up is the velocity of particles, μ is the dynamic viscosity of fluid, ρ is the density of fluid, ρp is the density of particles, and dp is the diameter of particles. Relative Reynolds number is also defined as equation (7):

$$Re = \frac{\rho d_p|\vec{u}_p - \vec{u}|}{\mu} \quad (7)$$

The Drag coefficient of CD is also calculated from equation 8 (for spherical particles):

$$C_D = a_1 + \frac{a_2}{Re} + \frac{a_3}{Re^2} \quad (8)$$

Where the coefficients a1, a2 and a3 are calculated from the relationship provided by [38] for different values of the Reynolds number.

3. Materials and Methods

In this study, two types of particles with strong and weak magnetic properties were used. Iron ore concentrate and iron ore tailing were prepared and the fractions of +180, +125, +90 and +63 microns were selected from the materials and were used for the experimental tests. The density of particles was determined by pycnometer (AccuPyc II 1340 | Micromeritics model). The magnetization of the particles (M) was measured using Hommade VSM. Magnetic flux density of the space around the magnetic sector of device (permanent magnet), at different distances and directions was also measured with the Gauss and Teslameter (F.W.Bell (SYPRIS) and Model 5170).

3.1. Separator device (Wet LIMS)

In the present study, a wet low intensity magnetic separator device (BOXMAG-Rapid Limited model) was used for simulation process and magnetic separation experimental tests. This device includes three main parts such as a magnetic cylinder, magnetic sector (consisting of permanent magnets placing in the cylinder in angle form), and tank (the main place of magnetic separation). It should be noted that in the device, magnets place in an axial arrangement. Besides, magnetic sector consists of three ferrite type (ceramic rectangular cube block magnets that the upper and bottom magnets are similar). In Fig. 1, schematic view of the magnetic separator device is shown. The cylindrical drum and separator tank are steel (316). The remaining flux density (with the Gaussian unit, which is a characteristic of the permanent magnet) for all three magnets was 1,500 gauss. In fact, the pulp containing strong-magnetic and weak-magnetic particles with a specified solid weight percentage will enter the path to the separator. The pulp then goes to the elemental portion of the separating tank in a narrower space, and in practice, the process of magnetic separation of the particles will take place. In this way, the magnetic particles in the pulp are attached to the cylinder of the machine (permanent magnets inside the cylinder absorbing magnetic particles to the cylindrical shell), and then moving the magnetic materials towards the concentrate output with the cylindrical rotation. In the outlet part, using the washing process, the magnetic particles adhering to the cylinder

Figure 1: View of the wet low intensity magnetic separator device (BOXMAG-Rapid model)

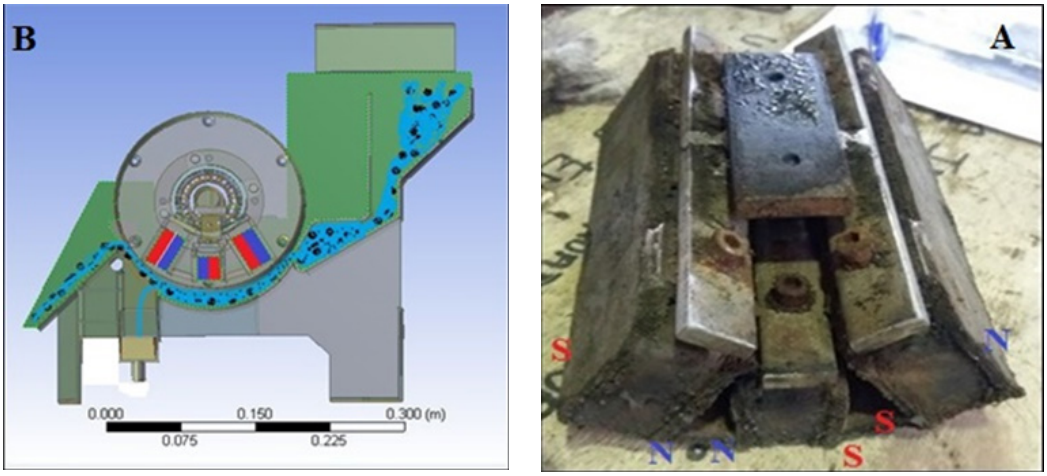

Figure 2: Depictions of the magnets and position of the N and S poles (A) and a schematic diagram of the pulp moving in a separator (B)

will be washed out of it. Weak-magnetic particles also move from the bottom of the tank to the tail output. In Fig. 2, depictions of the magnets and a schematic diagram of how the pulp moves in a separator is shown.

The maps of the magnetic sector, magnetic cylinder, and tank were prepared in SolidWorks software and then the creation of the corresponding mesh were performed in the ICEM- CFD software. Simulation of the magnetic variables was performed using FEM numerical modeling in the COMSOL Multiphysics simulator by the AC / DC module and the Magnetic Fields, No Currents option. In the next step, simulating the fluid flow of the particles, was done by using the Ansys Fluent simulator (DPM modeling).

3.2. General path of simulation

In order to simulate the process of magnetic separation; firstly, the magnetic field and the corresponding variables (including magnetic flux den-

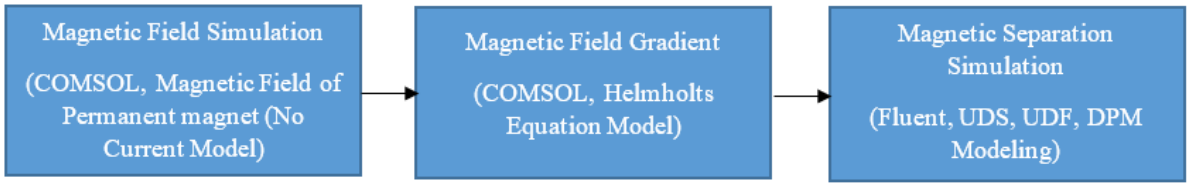

Figure 3: Arrangement of simulation steps of magnetic separation in the Wet LIMS device

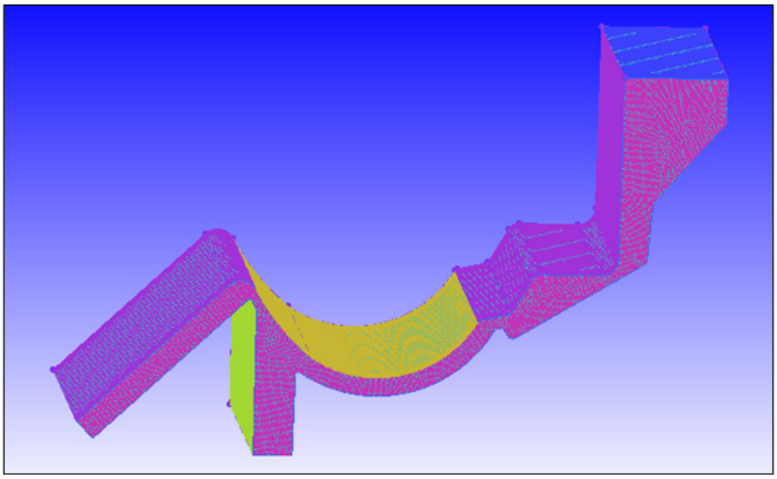

Figure 4: A schematic view of the Laboratory wet LIMS in the ICEM CFD software

sity (B) in terms of tesla and the magnetic field magnitude (H) in terms of ampere per meter), was simulated in the FEM based simulator. To generate the magnetic field gradient (∇H), the Helmholtz model was used. In the next step, the magnetic field gradient values were imported to the fluent simulator software using a user defined scalar (UDS). Then, in order to apply magnetic force on the particles, a user defined function (UDF) was used. In the last step of the simulation, in order to simulate the pulp flow, Lagrangian Discrete Phase Model (DPM) was applied. In Fig. 3, the simulation process performed in this research is shown schematically.

3.3. Model development

For mesh generation, various meshes have been produced using unstructured, structured and semi structured methods. The specification of the generated meshes shows that the highest number of cells is related to the fine unstructured mesh with 872,026 cells, which has an orthogonal quality index of 0.322. Furthermore, the semi-structured generated mesh has 495,400 cells, with its orthogonal quality index much higher than the fine unstructured mesh (0.514). In addition, the structured mesh has an orthogonal quality index of 0.360 (higher than the orthogonal quality index of a fine unstructured mesh) that has fewer cells (276024).

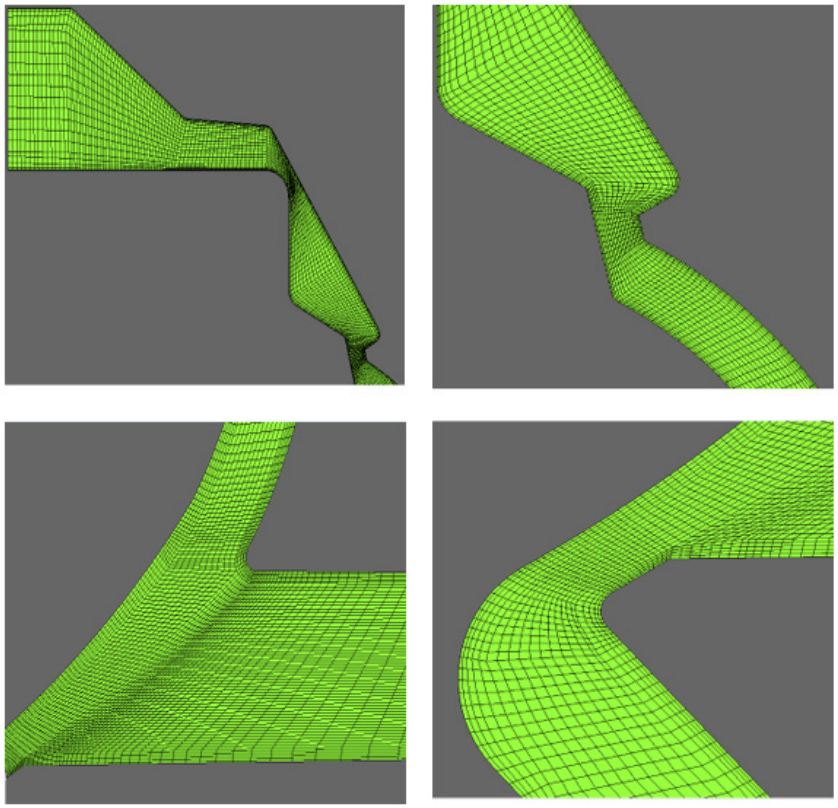

Figure 5: Exhibits of generated mesh in different parts of the separator device

It is necessary to mention that the inlet (for pulp flow inlet), the outlet (for tailing and concentrate outputs), and the rotational moving wall (for rotating drum of the device) were considered as the separation boundaries of the geometry. The number of cells, nodes and faces of the final selected mesh (with semi-structured method) were 495400, 328491, and 1322708 respectively. In the beginning of the simulation and in order to reach better convergence of the residual curve, only the flow of water inside the device was simulated in steady state. Then with these initial values, the simulation of injection of pulp (particles and water) was initiated. A schematic view of the Laboratory wet LIMS equipment in the ICEM CFD software environment is shown in In Fig. 4. Exhibits of generated mesh in different parts of the device (input, outputs of tailings and concentrate and separation tank) are also showed In Fig. 5.

In this simulation, the SIMPLE algorithm was used for coupling the velocity and pressure equations. Besides, the second-order upwind scheme was used for discretization of momentum and continuity equations and to solve kinetic energy of turbulence and turbulence dissipation rate. In order to achieve a convergent solution, the values of "under relaxation factors" for pressure, momentum and body forces were adjusted as 0.2, 0.5 and 0.5, respectively. Also, the under relaxation factor of 0.2 was applied to two variables of kinetic energy and the dissipation rate of turbulence. The time step of the simulation was equal to 0.05 and 0.0001 second for the particle and fluid respectively and the convergence criterion was considered to be 0.001. In Table 2, the parameters used in the simulation are briefed.

4. Results and discussion

4.1. Simulation of magnetic field

There is three materials including ferrite (ceramic) cuboid magnets, steel cylindrical drum and separator tank (steel 316), and air that cover around the magnets were used to simulate the magnetic field. In Fig. 6, a schematic view of the geometry created in the simulator, COMSOL Multiphysics, is shown. In the next step, the region related to the generation of the magnetic field should be determined. In addition, the generation power of the magnetic field was determined using remaining flux density variable (This value is equal to 1,500 gausses for each of the three magnets). This value should be applied in a particular direction, which is referred to as polarization direction and is determined by the poles N and S of the magnets. In the desired problem, this direction was determined after determining the poles of N and S of the magnets and the angle of the magnets with the

Table 2: Parameters used in the simulation of the magnetic separation process of particles

Parameter	Value
Magnetic particle density (Kg/m^3)	5020.0
None-magnetic particle density (Kg/m^3)	3215.7
Particle diameter (magnetic and none-magnetic) (micron)	125
Water density (Kg/m^3)	998.2
Water viscosity (Kg/m×s)	0.001003
External magnetic field (flux density, Tesla)	0.1T
Magnetization of magnetic particle (emu/gr)	64.6
Magnetization of none-magnetic particle (emu/gr)	4.4
Weight solid percent of the input pulp (%)	25
Mass flow rate of magnetic particles (Kg/s)	0.13
Mass flow rate of none-magnetic particles (Kg/s)	0.03

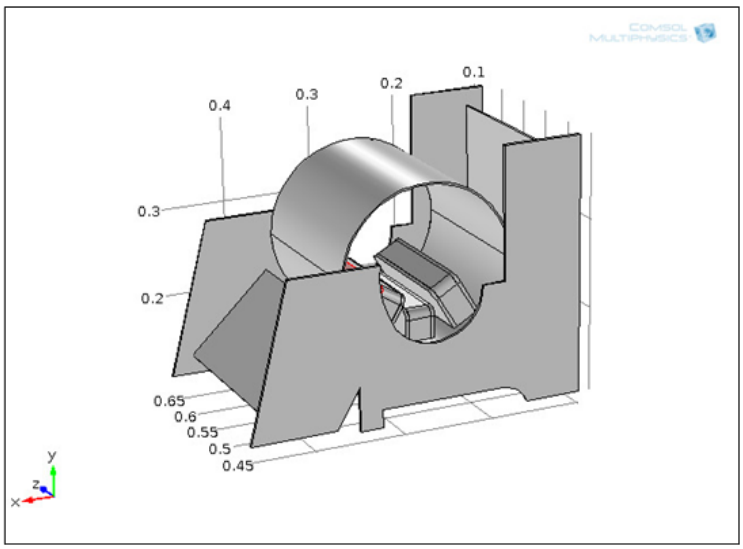

Figure 6: Schematic view of the created geometry of the wet LIMS in the COMSOL Multiphysics

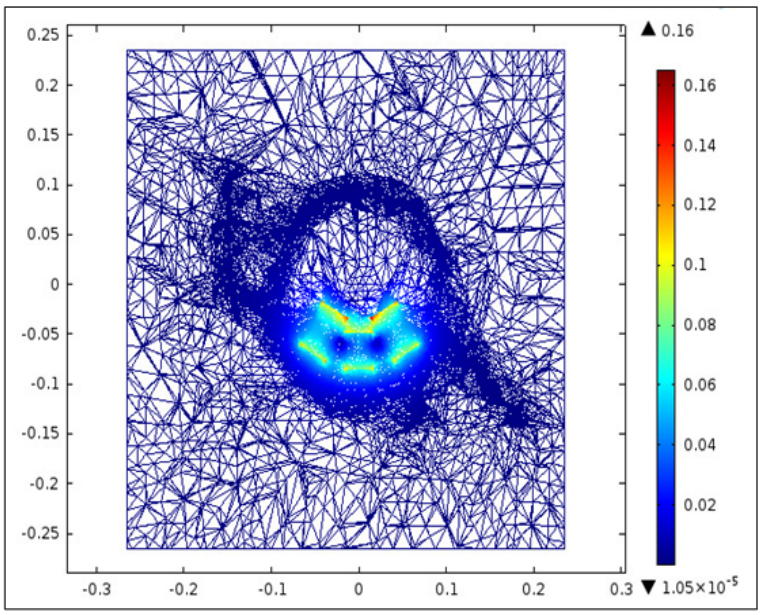

Figure 7: Schematic view of the created mesh with the magnetic flux density distribution in the device

horizon (X-axis) and shown in Fig. 2(A). Moreover, the magnetic insulation boundary condition was considered as surrounding cubic plates, which will limit the calculation of the magnetic field in this space. After these steps, the mesh of generated geometry in the simulator was produced with a specified limit for the size of elements (which is related to the problem physics). A view of the produced mesh is shown in Fig. 7.

Fig. 7 illustrates a view of the constructed mesh where the inlet of the separator is located on the left, and the rotating cylinder shell of the separator is further characterized by a blue circular dense mesh. In this figure, the position of the magnets is also determined and their color spectrum, according to the legend, indicates the distribution of the magnetic flux density in the space around the magnets. Triangular meshes were used so as to achieve better convergence and stability in the solution. After solving the physics of the problem, the graphical results of magnetic flux density was also shown in Fig. 7. As seen in Fig. 7, the value of the magnetic flux density on the magnet is 900 to 1000 gauss considering the legend in right side of Fig. 7.

4.2. validation of the simulation results of the magnetic field

In order to validate the simulation results of the magnetic field, the size of the magnetic field (in Gauss) was measured at 43 points around the mag-

netic sector using a gauss meter. Considered points were located in the middle section of the magnets and in 6 directions with different angles and different distances from the magnets (Fig. 8 (A)). The quantitative comparison of the measured and simulated magnetic field intensity at different points was also shown in Fig. 8. As seen in Fig. 8, the value of magnetic field intensity was reduced by the distance from the surface of the cylinder. This reducing trend was obvious in both laboratory measurement and the results of the simulation. On the other hand, the results of magnetic field simulation were in agreement with those of laboratory measurement. In general, the evaluation of Fig 8 showed that the quantitative results of magnetic field simulation were consistent with laboratory measurements and the maximum simulation error of 7.8% in different directions. It should be noted that the effective magnetic field in the surface of the drum shell and in the middle section of the magnets is about 1,000 Gauss (based on the simulation and measurement results, Fig 8).

4.3. Simulation of pulp flow in wet LIMS

To simulate of the pulp flow in the separator device, initially and by considering the viscous model of the standard k-ε, boundary conditions of the mass flow inlet, pressure outlet and rotating wall, for the pulp inlet of the separator, tailings and concentrates outputs, and the rotary cylinder of the separator, simulation was started to solve the flow of water inside the separator. After the conver-

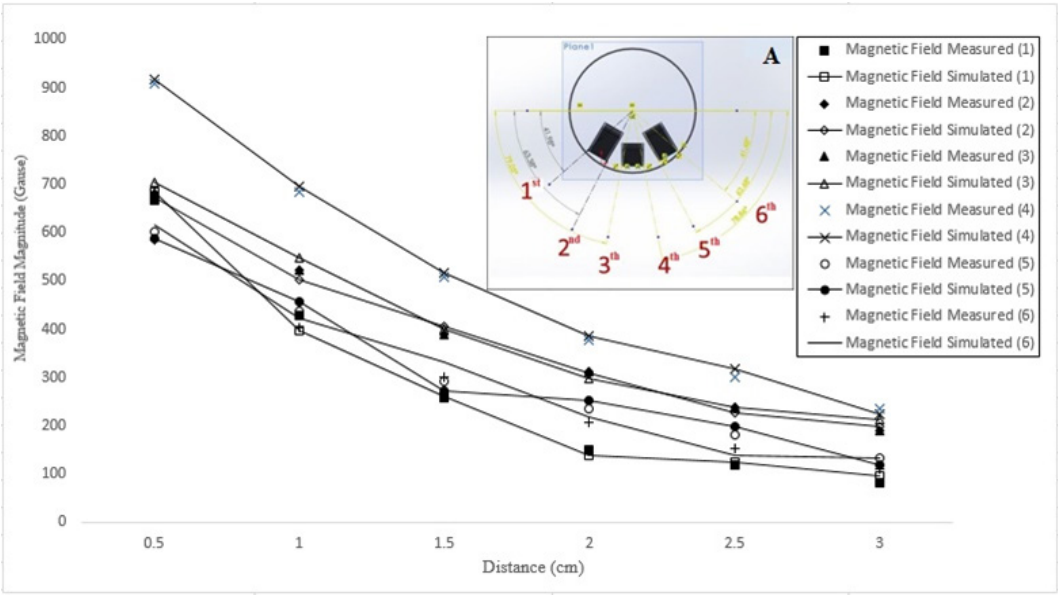

Figure 8: Measured and simulated values of magnetic field magnitude (gauss) in 6 directions (A) and different distance from the surface of the drum in the middle section of magnets

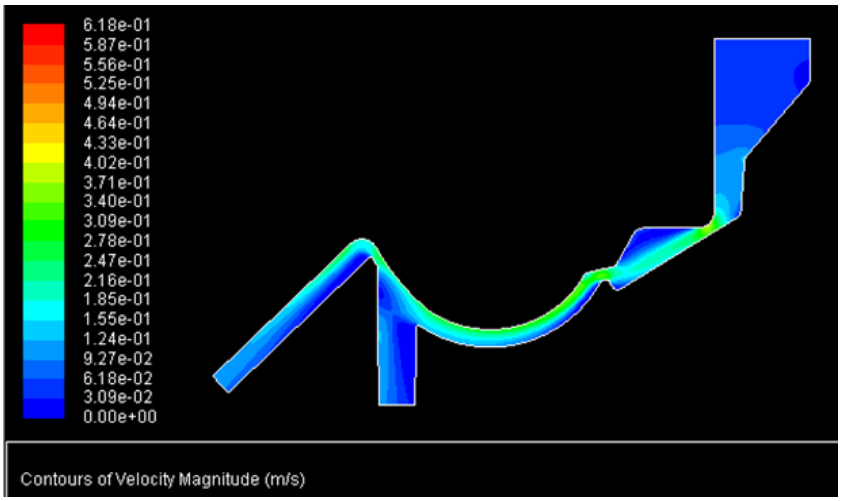

Figure 9: Water velocity values in different parts of the separator device

gence of the solution, the flow of water inside the separator was studied and, due to the existence of vortices in the device, finally the RNG k-ε model was selected for the viscous model of the simulation. At this stage, the velocity values of water in different parts of the separator were also investigated which are shown in Fig. 9.

After forming the solution of water flow inside the magnetic separator in the first stage of simulation, in the second step, by using the discrete phase Lagrangian model (DPM), a simulation of the pulp flow (solids and water) was performed. It must be noted that , at this stage, in addition to the drag and gravity forces, the magnetic force will also be applied (through the UDF code) on the particles. In the first stage of the simulation, the flow of water inside the separator was steady state and considering the turbulence model of k-ε type of RNG model. The simulation conditions in the second stage of the simulation are presented in Table 2. In the second step, simulating and injecting particles and fluid into the magnetic separator, the selected time step is important for particle tracking. The time step of a particle in tracking simulations is is calculated from equation 9 [39]:

$$\tau = \frac{Sd^2C_c}{18\vartheta} \quad (9)$$

In equation 9, S, the particle-to-fluid ratio, the Cunningham constant Cc, d, the particle diameter, and ϑ is kinematic viscosity of the fluid, which was obtained by calculating and applying stringent conditions, this time step for particle was achieved 0.0001 seconds.

After simulating the magnetic separation process in the separator device, the graphical outputs of the position of the particles are discussed below. In order to investigate the position of the particles more precisely, magnetic and none-magnetic particles are shown in separate images in the figures. The position of none-magnetic particles at times of 1.3, 1.8, 2.8, and 4.3 seconds is shown in Figure 10, and the position of the magnetic particles in these times is also shown in Figure 11.

The images of the position of the none-magnetic particles in different times (Fig. 10) showed that the particles did not absorb through the magnetic field of the shell after passing the inlet portion of the separating device and reaching the cylindrical portion, and moved towards the outlet of the none-magnetic materials, which has a perfect conformity with physical reality of the separation test. This is while magnetic particles absorbed towards the magnetic field of the cylinder shell after entering the separating device, and over time, the density of magnetic particles in the cylindrical part increased (Fig. 11). There is a slight difference between the positions of magnetic and none-magnetic particles up to about 1.3 seconds (Figures 10 (A) and 11 (A)). But this difference in the positioning of particles at 1.8 seconds (Figures 10 (B) and 11 (B)) is clearly visible. So that the none-magnetic particles have more forward motion, this is where magnetic particles are concentrated in the primary portion of the magnetic cylinder. This shows the influence of magnetic particles from magnetic force. An issue that has substantially less impact on none-magnetic particles. The curvilinear motion of the none-magnetic particles towards the tailing output starts at 2.8 seconds (Fig. 10 (C)). At the same time, however, the magnetic particles are quite prominent and are completely subjected to the magnetic force of the magnetic cylinder (Fig. 11 (C)). Meanwhile, an increase in the residence time of the magnetic particles (towards the red color) is observed in this figure and later figures.

At simulation time of 4.3 seconds (Fig. 10 (D)), the aggregation of none-magnetic particles in the tailings output is increasing, which is a consequence of the increasing trend in subsequent simulations. It seems that the behavior of the none-magnetic particles and their position at different times within the magnetic separator is largely simulated correctly. At 4.3 seconds, the position of magnetic particles (Fig. 11 (D)) is perfectly within the area of the influence of the magnetic field (magnetic cylinder). By examining the subsequent simulation times, it is determined that a large part of the none-magnetic particles are moving in their proper direction and toward the tailings output. But in addition, some particles are none-magnetic (with a lower percentage) that their path is moving in the direction of the second outlet (the concentrate output). In addition to the none-magnetic particles moving toward the concentrate output, there are some magnetic particles which are moving towards the tailings outlet. But the amount of magnetic particles that move towards the tailings outlet is less than the none-magnetic particles that move toward the concentrate outlet.

4.4. validation of the pulp flow simulation results

After the general trend of magnetic and none-mag-

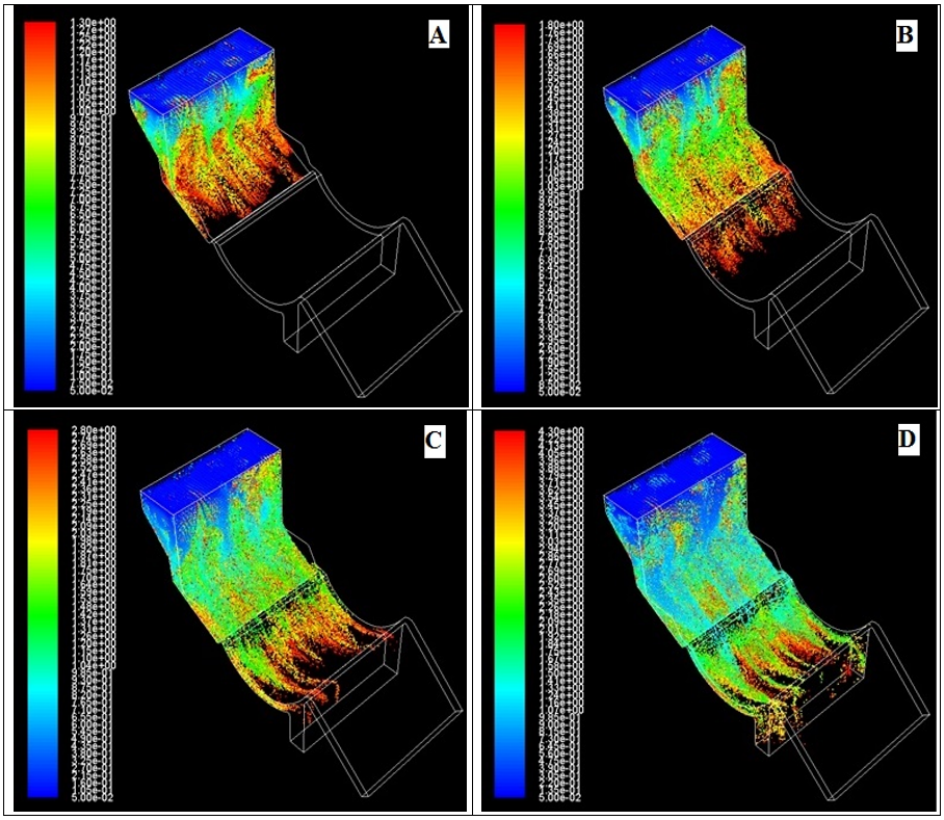

Figure 10: Simulation of the position of none-magnetic particles inside the magnetic separator device at 1.3 (A), 1.8 (B), 2.8 (C) and 4.3 seconds (D)

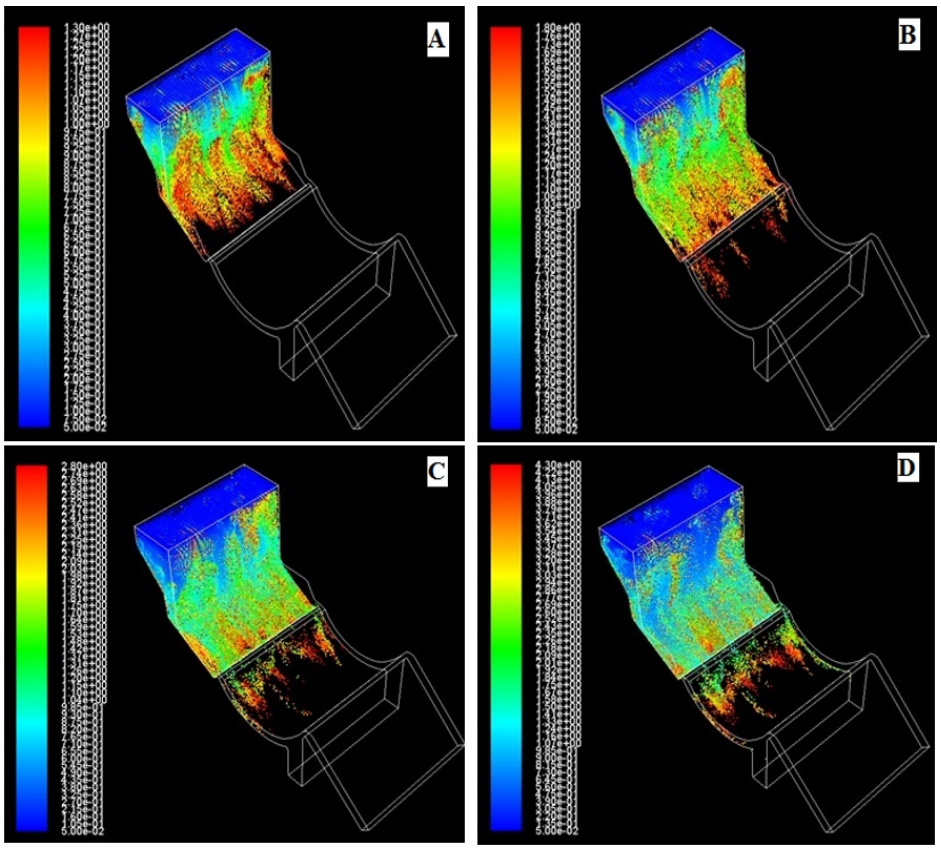

Figure 11: Simulation of the position of magnetic particles inside the magnetic separator device at 1.3 (A), 1.8 (B), 2.8 (C) and 4.3 seconds (D)

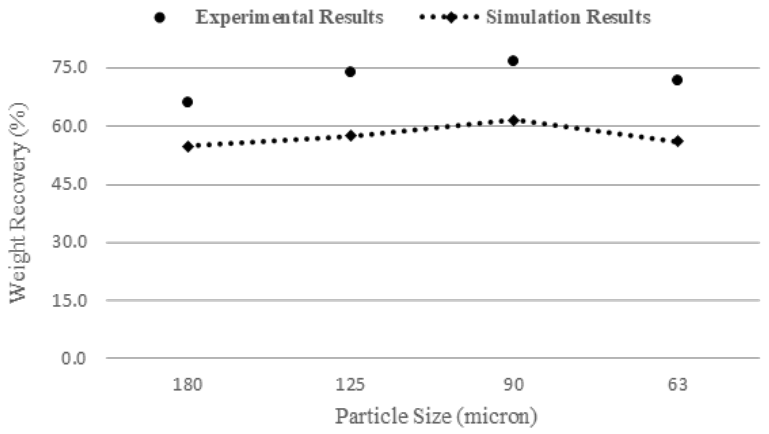

Figure 12: Experimental and appropriate simulations results of the magnetic separation tests in different particle size of the input pulp feed

netic particles flow during the simulation with the reality of the magnetic separation test in the wet LIMS machine was qualitatively consistent, in the next step, in order to compare the results of the simulation and magnetic separation test quantitatively (validation of simulation results), a laboratory test was carried out under the simulation conditions (the solid percent of input pulp was 25 wt.% and the size of the pulp particles (magnetic and non-magnetic particles) was 125 microns). The simulation time was 10 seconds. During the simulation, sampling was done from tailings and concentrates outputs, as well as trapped particles into a rotating cylinder. Then, the simulation results were compared with the experimental results. Given the fact that the main response of magnetic separation test is the recovery of magnetic particles (that absorbing to the rotating drum), this amount is compared with each other after the experiment and simulation. The value of magnetic recovery in the laboratory test was 74% and this value was 55.57% after the simulation. The difference between the results of the simulation and the magnetic separation test was 16.45%. Therefore, it seems that the magnetic separation test has been simulated acceptably.

4.5. Simulations and validations of the particle size and solid percentage of the input pulp

In order to quantify the results of the simulation, magnetic separation simulation was performed by changing two variables affecting the magnetic separation process and corresponding experiments (variables of particle size of input pulp feed particles consist of four levels (+180, +125, +90 and +63 microns) and solid percentage of the input pulp in four levels of 15, 20, 25 and 30 % by weight which the results are shown in Figure 12 and 13.

As shown in Figure 12, the trend of the simulation results is consistent with the laboratory results of weight recovery, with the highest weight recovery in the size of 90 microns in simulation (61.65 %) and experimental (76.7 %) results. The highest simulation error was in the size of 125 micron (16.5%) and the lowest simulation error was

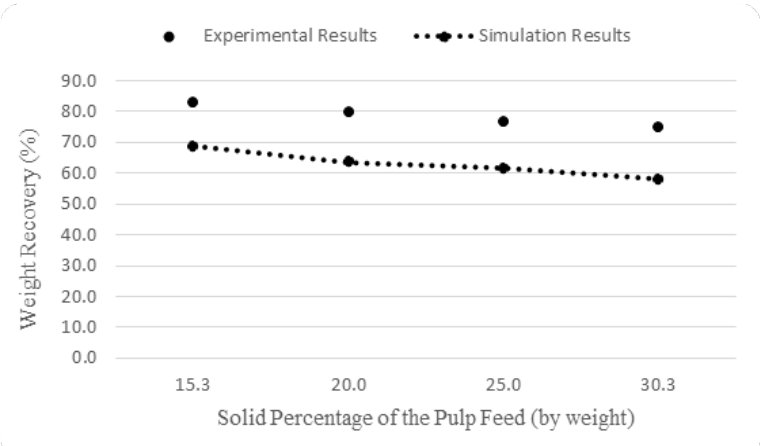

Figure 13: Experimental and appropriate simulations results of the magnetic separation tests in different solid percentage of the pulp feed

in the size of 180 micron (11.4%). Examination of the simulation trend has shown that by reducing the particle size (magnetic and non-magnetic), the percentage of non-magnetic particles (which must be removed from the tail path) has a completely decreasing trend.

As can be seen in Figure 13, the weighted recovery response trend of the magnetic separation test is the same in the different solid percentages of the input pulp in the experiments as well as the simulation results. The lowest simulation error in predicting weight recovery in the solid percentage of 15% (equivalent to 14%) and the highest simulation error in the solid percentage of 30% (equivalent to 16.9%). It seems that as the solid percentage of the pulp increases, the viscosity of the pulp increases, and as a result, the effect of the fluid drag force on the separation process decreases, leading to a reduction in the weight recovery. It seems that the path of magnetic and non-magnetic particles and their positions inside the separator in the process of magnetic separation and the response of the weight recovery to magnetic separation test (as a quantitative result) are acceptable by using of this simulation method.

5. Conclusion

In this research, the magnetic separation process of particles in the wet LIMS equipment was simulated by combining the numerical methods of FEM for simulation of the magnetic field variables and CFD for simulation of the pulp flow enhanced by DPM model for particle tracking. In the first step of this research, the results of simulation and laboratory measurements of the magnetic field magnitude indicated that the maximum percentage of simulation error was 7.8% in various directions. Generally, the comparison of simulation results and laboratory measurements of magnetic field confirmed that the quantitative results of magnetic field simulation were consistent with laboratory measurements. In the continue, simulation of pulp flow and tracking the magnetic and none-magnetic particles, as the second step of the simulation, was done. After confirming the qualitative results of simulation and correct tracking position of magnetic and none-magnetic particles, in order to validation of simulation results quantitatively, the magnetic separation experimental tests (by changing two variables of particle size of the input pulp feed particles and solid percentage of input pulp) were carried out according to the simulation conditions. The maximum difference between the results of the simulation and the magnetic separation experimental tests (recovery of magnetic particles in the concentrate product) was 16.9%. This comparison, showing the capability of the combining approach to confront the simulation of systems with the base of magnetic separation. Furthermore, it also could be concluded that in the operating conditions similar to levels of variables of this study, DPM approach could be well suited for simulation, designing and constructing more developed magnetic separators with higher efficiencies.

Acknowledgments

This work was supported by the Iranian Mines & Mining Industries Development & Renovation (IMIDRO), Iran Mineral Processing Research Center (IMPRC), Gol-Gohar Mining and Industrial Company (GEG) and Golgohar Iron ore and Steel Research Institute (GISRI). We are grateful to Dr. Soltan Mohammadi, Mr. Badraghe and Mr. Salmaniye in IMPRC, for facilities, scientific and technical assistance. We also wish to thank Mr. Hajizadeh and Ghorbannejad for their contributions to the work reported in this paper.

Refrences

1. Mohanty, S., Das, B., & Mishra, B. K. (2011). A preliminary investigation into magnetic separation process using CFD. Minerals Engineering, 24(15), 1651-1657.

2. Yavuz, C. T., Prakash, A., Mayo, J. T., & Colvin, V. L. (2009). Magnetic separations: from steel plants to biotechnology. Chemical Engineering Science, 64(10), 2510-2521.

3- Das, B., Prakash, S., Bhaumik, S. K., Mohapatra, B. K., & Narasimhan, K. S. (1991). Magnetic separation of iron ore slimes by wet high intensity magnetic separator. Transactions of the Indian Institute of Metals (India), 44(5), 355-357.

4. Song, S., Lu, S., & Lopez-Valdivieso, A. (2002). Magnetic separation of hematite and limonite fines as hydrophobic flocs from iron ores. Minerals engineering, 15(6), 415-422.

5. Arol, A. I., & Aydogan, A. (2004). Recovery enhancement of magnetite fines in magnetic separation. Colloids and Surfaces A: Physicochemical and Engineering Aspects, 232(2-3), 151-154.

6. Chen, L., Xiong, D., & Huang, H. (2009). Pulsating high-gradient magnetic separation of fine hematite from tailings. Mining, Metallurgy & Exploration, 26(3), 163-168.

7. Tripathy, S. K., Banerjee, P. K., & Suresh, N. (2014). Separation analysis of dry high intensity induced roll magnetic separator for concentration of hematite fines. Powder Technology, 264, 527-535.

8. Bertrand C, Bazin C, Nadeau P (2018) Simulation of a Dry Magnetic Separation Plant. Advances in Metallurgical and Material Engineering, 1(1):15-28.

9. Svoboda, J. (2004). Magnetic techniques for the treatment of materials. Springer Science & Business Media.

10. Iranmanesh, M., & Hulliger, J. (2017). Magnetic separation: its application in mining, waste purification, medicine, biochemistry and chemistry. Chemical Society Reviews, 46(19), 5925-5934.

11. Norrgran, D. (2010). Wet Drum Magnetic Separators for Heavy Media Application, Operation, and Performance. In XVI International Coal Preparation Congress, Lexington: Society for Mining, Metallurgy, and Exploration (pp. 313-319).

12. Chen, L., Liao, G., Qian, Z., & Chen, J. (2012). Vibrating high gradient magnetic separation for purification of iron impurities under dry condition. International Journal of Mineral Processing, 102, 136-140.

13. Jordens, A., Sheridan, R. S., Rowson, N. A., & Waters, K. E. (2014). Processing a rare earth mineral deposit using gravity and magnetic separation. Minerals Engineering, 62, 9-18.

14. Zhang, W., Rezaee, M., Bhagavatula, A., Li, Y., Groppo, J., & Honaker, R. (2015). A review of the occurrence and promising recovery methods of rare earth elements from coal and coal by-products. International Journal of Coal Preparation and Utilization, 35(6), 295-330.

15. Augusto, P. A., Castelo-Grande, T., & Augusto, P. (2005). Magnetic classification in health sciences and in chemical engineering. Chemical Engineering Journal, 111(2-3), 85-90.

16. Alexiou, C., Arnold, W., Klein, R. J., Parak, F. G., Hulin, P., Bergemann, C., & Luebbe, A. S. (2000). Locoregional cancer treatment with magnetic drug targeting. Cancer research, 60(23), 6641-6648.

17. Svoboda, J., & Fujita, T. (2003). Recent developments in magnetic methods of material separation. Minerals Engineering, 16(9), 785-792.

18. Dobbins, M., Dunn, P., & Sherrell, I. (2009, September). Recent advances in magnetic separator designs and applications. In The 7th International Heavy Minerals Conference "What next", The Southern African Institute of Mining and Metallurgy (pp. 63-70).

19. Stener, J. (2015). Wet Low-Intensity Magnetic Separation: Measurement methods and Modelling (Doctoral dissertation, Luleå tekniska universitet).

20. Dworzanowski, M. (2010). Optimizing the performance of wet drum magnetic separators. Journal of the Southern African Institute of Mining and Metallurgy, 110(11), 643-653.

21. Mohanty, S., et al. (2014) A CFD study of a magnetic separator with sphere matrix. XXVII International Mineral Processing Congress 2014, Santiago, Chile, 64-72.

22. Sido, N.M., et al. (2003) Study of high intensity magnetic separation process in grooved plate matrix. Eur. Phys. J. Appl. Phys. 24, 201–207.

23. Okada, H., et al. (2005) Computational fluid dynamics simulation of high gradient magnetic separation. Separation Science and Technology, 40(7), 1567–1584.

24. Hayashi, S., et al. (2010) Development of high gradient magnetic separation system for removing the metallic wear debris to be present in highly viscous fluid. Physica C: Superconductivity 470(20): 1822-1826.

25. Lindner, J., et al. (2013) Simulation of magnetic suspensions for HGMS using CFD, FEM and DEM modeling. Computers & Chemical Engineering 54(0): 111-121.

26. Shaikh, S., et al. (2016) Study on Optimizing High-Gradient Magnetic Separation- Part 1: Improvement of Magnetic Particle Retention Based on CFD Simulations. World Journal of Condensed Matter Physics, 6, 123–136.

27. Sejja, K., et al. (2011) Computational Fluid Dynamics Simulation of a Quadrupole Magnetic Sorter Flow Channel: Effect of Splitter Position on Nonspecific Crossover. Can J Chem Eng, 89(5): 1068–1075.

28. Murariu, V. (2013) Simulating a low intensity magnetic separator model (LIMS) using DEM, CFD and FEM magnetic design software. Proceedings of Computational Modelling 2013, Falmouth, UK. 1-14.

29. Wang, F., Zhao, H., Dai, H., & Du, W. (2019). Fully coupled multi-physics modeling of the multi-type magnetic particles dynamic behavior in low intensity magnetic separator. Physicochemical Problems of Mineral Processing, 55.

30. Zhe, J. I. N., Xin, T. A. N. G., & WANG, W. M. (2006). A Method for Shimming a Permanent Magnet with FEA. Journal of Iron and Steel Research, International, 13, 423-426.

31. LIU, J. F., Choi, H., & Walmer, M. (2006). Design of permanent magnet systems using finite element analysis. Journal of Iron and Steel Research, International, 13, 383-387.

32. Lozin, A. A., Nitiagovsky, V. V., & Hud, V. N. (2006). Magnetic System with "Antiradial" Magnetization. Journal of Iron and Steel Research, International, 13, 471-473.

33. Wimmer, G., Clemens, M., & Lang, J. (2008). Calculation of magnetic fields with finite elements. In From Nano to Space (pp. 111-124). Springer, Berlin, Heidelberg.

34. Manz, B., Benecke, M., & Volke, F. (2008). A simple, small and low cost permanent magnet design to produce homogeneous magnetic fields. Journal of magnetic resonance, 192(1), 131-138.

35. U.S. Patents., (2013). "Multiphysics Modeling using COMSOL",. Available at www.comsol.com/product-download.

36. Luo, L., & Nguyen, A. V. (2017). A review of principles and applications of magnetic flocculation to separate ultrafine magnetic particles. Separation and Purification Technology, 172, 85-99.

37. Fluent Inc., (2013) Fluent 14.5 users' guide, modeling multiphase flows Fluent Inc. Centerra Resource Park 10, Cavendish Court Lebanon, NH 03766.

38. Morsi, S., & Alexander, A. J. (1972) An investigation of particle trajectories in two-phase flow systems. Journal of Fluid Mechanics, 55(2), 193-208.

39. Ahmadi, G. (2005, June). "Particle Transport, Deposition and Removal", A Combined Research and Curriculum Development Project. In 2005 Annual Conference (pp. 10-986).